Chapter 7

Fluorescence Imaging of Single Kinesin Motors on Immobilized Microtubules

Till Korten, Bert Nitzsche, Chris Gell, Felix Ruhnow, Cécile Leduc, and Stefan Diez

Abstract

Recent developments in optical microscopy and nanometer tracking have greatly improved our understanding of cytoskeletal motor proteins. Using fluorescence microscopy, dynamic interactions are now routinely observed in vitro on the level of single molecules mainly using a geometry, where fluorescently labeled motors move on surface-immobilized filaments. In this chapter, we review recent methods related to single-molecule kinesin motility assays. In particular, we aim to provide practical advice on: how to set up the assays, how to acquire high-precision data from fluorescently labeled kinesin motors and attached quantum dots, and how to analyze data by nanometer tracking.

Key words: Kinesin, Single molecule, Imaging, TIRF microscopy, Motor protein, Microtubule

1. Introduction

In vitro motility assays, where the movement of molecular motors along surface-bound cytoskeletal filaments is imaged by optical methods, have greatly improved our understanding of the mechanochemical properties of motor proteins. First, such assays were performed by binding the motors to large, micron-sized beads, which could be followed by video microscopy (1–3) or held in an optical trap (4–6). Later on, Funatsu et al. pushed the sensitivity of the fluorescence microscope to the limit of being able to visualize individual motor molecules labeled with cyanine-based fluorophores (7). Using total internal reflection fluorescence (TIRF) microscopy, the processive movement of individual kinesin-1 molecules along microtubules was visualized by labeling the motors with Cy3 (8) or with green fluorescent protein (GFP) (9). Since then, the number of single-molecule fluorescence measurements of kinesin and dynein motors interacting with

Erwin J.G. Peterman and Gijs J.L. Wuite (eds.), *Single Molecule Analysis: Methods and Protocols*,
Methods in Molecular Biology, vol. 783, DOI 10.1007/978-1-61779-282-3_7,

microtubules has vastly expanded. Nowadays, not only the stepping of motors is observed in these assays, but also diffusion, (de)polymerizing activities of motors (and other microtubule-associated proteins), as well as interactions between motors and other proteins on the microtubule lattice (10–19).

In this chapter, we describe protocols for the imaging of single kinesin-1 molecules stepping along surface-immobilized microtubules using TIRF microscopy. These procedures should be understood as examples that need to be adapted in order to work for other motors or filaments (see also Notes 17 and 24). As the name indicates, TIRF microscopy excites fluorophores using light that is totally internally reflected at the interface of two materials with different refractive indices (e.g., glass and buffer). This reflected light produces an electromagnetic near field (termed "evanescent field") that decays exponentially with a decay length of 50–200 nm into the material with lower refractive index (see Fig. 1, left panel; for reviews, see refs. 20–23). A low penetration depth ensures that only fluorophores are excited which are very close to the surface. This "optical sectioning" reduces the background noise caused by molecules diffusing freely in solution, thus allowing the imaging of single fluorescent molecules. Due to the sensitivity of this fluorescence technique, it is essential to use clean glass surfaces that can be passivated efficiently (Subheading 3.2). Microtubules that self-assemble in vitro (Subheading 3.1) can be attached to these surfaces via antibodies

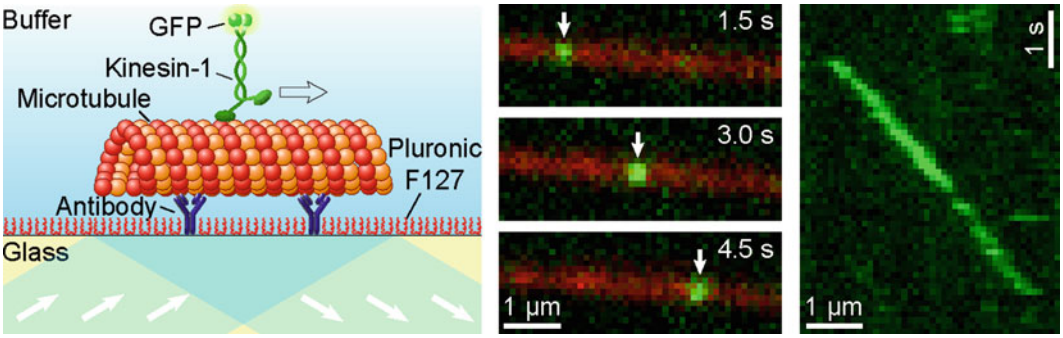

Fig. 1. Imaging single GFP-labeled kinesin-1 molecules moving along microtubules. *Left*: Schematic drawing of the assay. Microtubules are bound to a passivated glass surface with anti-tubulin antibodies. Single GFP-labeled kinesin-1 motors are imaged using the evanescent field generated by a totally internally reflected laser beam. *Middle*: Three frames of an image sequence showing a single kinesin-1 molecule (indicated with *arrows*) moving along a microtubule. *Right*: Kymograph of the same image sequence (microtubule not shown). Time progresses downward while the horizontal axis represents the distance along the microtubule. To record this data, we used an inverted fluorescence microscope (Zeiss Axiovert 200 M, Zeiss, Jena, Germany) with a commercially available TIRF-slider and an alpha Plan-Apochromat 100× oil 1.46 NA DIC objective (both Zeiss). Fluorescence signals were recorded using an EMCCD camera (Ixon DV 897, Andor, Belfast, N. Ireland). Excitation was achieved using either a mixed gas argon-krypton laser (Innova 70C Spectra; Coherent, Santa Clara, CA) or a liquid-waveguide coupled Lumen 200 metal arc lamp (Prior Scientific Instruments Ltd., Rockland, MA). Image acquisition and basic data processing were done using MetaMorph (Universal Imaging, Downingtown, PA).

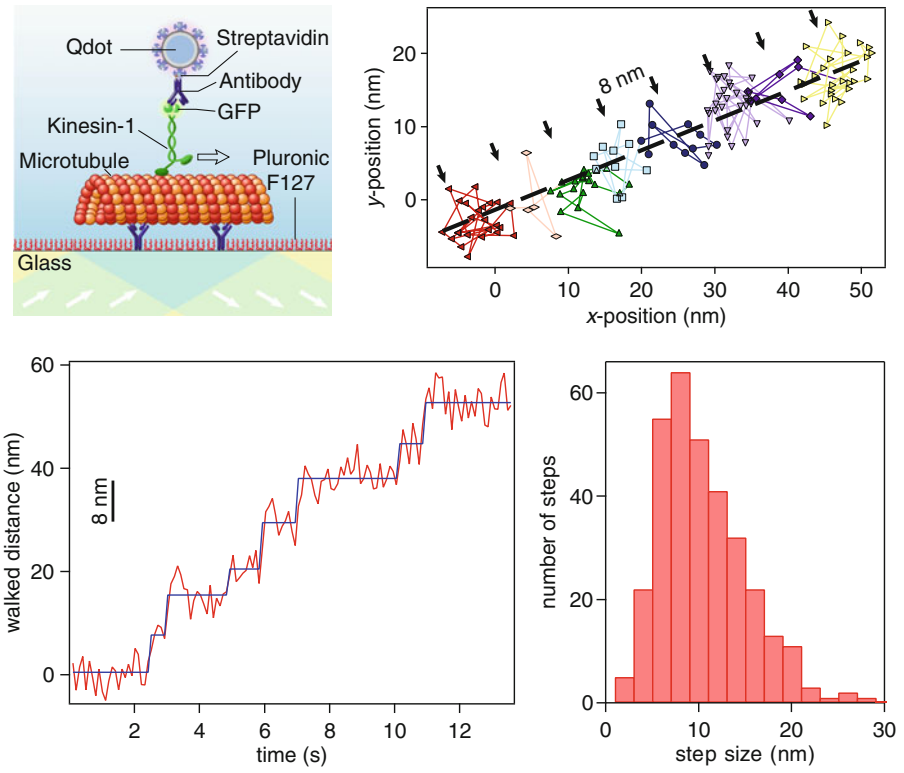

Fig. 2. Resolving 8 nm steps of a single kinesin-1 molecule using TIRF microscopy. *Top-left*: Schematic drawing of the assay. In addition to the assay explained in Fig. 1, a streptavidin-coated Qdot is attached to the kinesin-1 molecule via a biotinylated anti-GFP antibody. *Top-right*: Tracked *x*–*y* data of the Qdot positions. The *dashed line* indicates the average path of the Qdot. *Bottom-left*: Walked distance of the Qdot projected onto its average path plotted against time. Steps identified by a step-finding algorithm (47) are overlaid. *Bottom-right*: Histogram of step sizes identified by the step-finding algorithm (data from 12 molecules). The imaging setup used to acquire this data was the same as that was used for Fig. 1.

(Subheading 3.3). Single GFP- or quantum dot (Qdot)-labeled, truncated kinesin-1 molecules can then be observed moving along these microtubules. Using Gaussian model-based tracking algorithms, the position of these molecules can be localized with higher precision than the resolution of an optical microscope (24–28). With bright fluorescent labels, it is possible to resolve 8 nm steps of kinesin-1 (Fig. 2) and even smaller steps produced by two motors working collectively (29).

2. Materials

2.1. In Vitro Polymerization of Microtubules

1. BRB80: 80 mM Piperazine-*N*,*N*′-bis(2-ethanesulfonic acid) (PIPES), pH 6.9, with KOH, 1 mM ethylene glycol tetraacetic acid (EGTA), 1 mM $MgCl_2$.
2. Microtubule polymerization mix: BRB80 supplemented with 24% μl DMSO, 20 mM $MgCl_2$, and 5 mM GTP.

3. Tubulin, bovine (Cytoskeleton Inc, Denver, CO; unlabeled #5.11.2146; rhodamine labeled #5.11.2148). Store at −80°C. Stable for ~6 months.
4. Taxol (Paclitaxel; Sigma-Aldrich, Steinheim, Germany, #T7191): Dissolve to a final concentration of 100 mM in DMSO. Store 10-µl aliquots at −20°C. Stable for at least 1 year.
5. BRB80T: Dilute Taxol to a final concentration of 10 µl in BRB80.

2.2. Preparation of the Sample Chambers

1. Coverglasses 18 × 18 mm and 22 × 22 mm (Menzel, Braunschweig, Germany, #BB018024A1 and #BB022022A1, ask for thickness 1.5!).
2. Soap bath: 2% Mucasol in water.
3. Acetone.
4. Ethanol.
5. Nanopure water (>18 MΩ/m).
6. Piranha solution: Carefully mix 30% H_2O_2 with 97% H_2SO_4 at a ratio of 1:2 in a suitable container.
7. 0.1 M KOH in nanopure water.
8. Trichloroethylene (TCE)/dichlorodimethylsilane (DDS) solution: 0.05% DDS in TCE. Add TCE first, and stir while adding DDS to TCE (see Note 9). Prepare freshly in the clean container used for cover glass treatment (see Subheading 3.2.4).
9. Methanol.
10. Nescofilm (Roth, Karlsruhe, Germany, #2569.1).

2.3. Surface Passivation and Microtubule Binding

1. Tetraspeck fluorescent microspheres (0.2 µm, Invitrogen, Carlsbad, CA, #T7280): 1:100 dilution in BRB80 (see Subheading 2.1).
2. Anti-beta-tubulin antibody, SAP4G5 (Sigma-Aldrich, Steinheim, Germany, #T7816): Typically, a 1:200 to 1:1,000 dilution in BRB80 is used (see Note 16). The undiluted stock is stored at 4°C for several weeks.
3. F127 solution: 1% Pluronic F127 (Sigma-Aldrich, Steinheim, Germany, #P2443) is dissolved in BRB80 overnight, filtered (0.22-µm syringe filter), and stored at 4°C. Stable for ~6 months.
4. BRB20: 20 mM PIPES, pH 6.9, with KOH, 1 mM EGTA, 1 mM $MgCl_2$.
5. BRB20T: 10 µM Taxol (see Subheading 2.1) in BRB20.

2.4. Imaging GFP-Labeled Kinesin-1 Motors

1. Casein (Sigma-Aldrich, Steinheim, Germany, #C7078): Add 35 ml BRB80 (see Subheading 2.1) to 1 g casein in a 50-ml Falcon tube. Place the Falcon tube in a rotating wheel at 4°C and allow the casein to dissolve overnight. Let the large precipitates sediment in the Falcon tube placed upright. Centrifuge the supernatant at 10,000 × *g* at 4°C for 5 min. Filter the supernatant using a 0.22-μm syringe filter. Determine the concentration by measuring the absorbance at 280 nm. Dilute to the desired concentration (e.g., 10 mg/ml), snap freeze 40-μl aliquots in liquid nitrogen, and store at −20°C. Stable for at least 1 year.
2. GFP kinesin-1: We use truncated, GFP-labeled kinesin-1 constructs (rkin430GFP), which consist of the first 430 amino acids of kinesin-1 fused to a GFP and a his-tag at the tail domain. Cloning and purification have been described (30).
3. Antifade solution (see Notes 20–24): Supplement BRB20T (see Subheading 2.3) with final concentrations of 10 μM Taxol (see Subheading 2.1) and antifade reagents: 40 mM D-glucose, 160 μg/ml glucose oxidase (SERVA Electrophoresis GmbH, Heidelberg, Germany, #22778), 20 μg/ml catalase (Sigma-Aldrich, Steinheim, Germany, #C40), and 10 mM 1,4-dithio-DL-threitol (DTT).
4. Motor solution: Add final concentrations of 100 μg/ml casein, 1 mM ATP, and 50–500 pM GFP kinesin-1 to the antifade solution (see Notes 24 and 25).

2.5. Imaging Quantum Dot-Labeled Kinesin Motors

1. Biotinylated anti-GFP antibodies (produced by our antibody facility in-house): Biotinylated using EZ-Link NHS-PEO Solid Phase Biotinylation Kit (Pierce, Rockford, IL, #21450).
2. Qdots 655, streptavidin-coated quantum dots, emission peak at 655 nm (Invitrogen, Carlsbad, CA, #Q10121MP). Store at 4°C. Stable for ~1 year.

3. Methods

3.1. In Vitro Polymerization of Microtubules

Microtubules are commonly reconstituted from purified tubulin. Their physical structure, including the number of protofilaments and the stiffness, strongly depends on the assembly conditions (31–33). Below, we describe the production of stabilized (i.e., nondynamic) microtubules using GTP and the microtubule-stabilizing drug Taxol (see Note 1).

1. Add 1.25 μl of microtubule polymerization mix to 5 μl of 4 mg/ml tubulin in BRB80 (containing 3–25% rhodamine-labeled tubulin, see Note 2).

2. Incubate at 37°C for 30 min to allow microtubule assembly.
3. Dilute assembled microtubules by adding 493.75 µl of BRB80 supplemented by 10 µM Taxol and store them for up to 1 week at room temperature (see Notes 1 and 3).
4. Immediately before using the microtubules, centrifuge 50 µl of the microtubule solution at 100,000 × *g* for 5 min and resuspend (see Note 4) in 200 µl of BRB80T (final tubulin concentration ~100 nM).

3.2. Preparation of the Sample Chambers

Clean, low-fluorescence glass surfaces are essential for single-molecule TIRF microscopy of kinesin motors. Formed into simple flow cells, these glass surfaces allow convenient perfusion of solutions for immobilization of microtubules and introduction of kinesin. Unwanted nonspecific adsorption of fluorescent motors can be effectively prevented by surface passivation.

3.2.1. Cover Glass Precleaning

1. Place an equal number of 18 × 18-mm and 22 × 22-mm cover glasses into Teflon racks, ensuring that adjacent cover glasses cannot contact.
2. Sonicate for 15 min in a soap bath; rinse in deionized water for 1 min.
3. Bathe, sequentially, in acetone for 10 min, ethanol for 10 min, and nanopure water for 1 min.

3.2.2. "Piranha Solution" Cleaning

1. Transfer the cover glasses directly from the water bath to Piranha solution. Bathe for 1 h, heating the solution to 60°C. Extreme caution should be used, as Piranha solution is highly corrosive and potentially explosive (see Note 5).
2. Transfer racks directly from the Piranha solution sequentially to three nanopure water baths, bathing for 1 min each (see Notes 6 and 7).

3.2.3. Activating OH Groups on the Glass Surface for Silanization Using KOH

1. Transfer racks from the third nanopure water bath to a 0.1 M KOH bath for 15 min.
2. Transfer racks sequentially through two nanopure water baths, bathing in each for 1 min.
3. Remove from water bath and dry cover glasses completely with clean nitrogen gas (see Note 8).

3.2.4. Glass Silanization

1. Gently place the cover glasses into a container filled with TCE/DDS solution so that the glasses are completely immersed; bathe for 1 h.
2. Transfer the silanized glass, sequentially, through three methanol baths, placed in an ultrasonic bath for times of 5, 15, and 30 min.

3. Remove from the final methanol bath and dry cover glasses completely with clean nitrogen gas. Store in clean, sealed glass containers (see Notes 10 and 11).

3.2.5. Sample Chamber Assembly and Use

1. Cut out several small (30 × 2 mm) Nescofilm strips using a (razor) blade (see Notes 12 and 13).
2. Arrange the Nescofilm strips on one side of a silanized 22 × 22-mm cover glass, forming a series of parallel channels (up to 4), and cut off (using a razor blade) those parts of the strips that protrude over the edges of the cover glass.
3. Place an 18 × 18-mm silanized cover glass on top, sandwiching the Nescoflm strips.
4. Transfer the assembly (22 × 22-mm cover glass facing down) to a hot plate at a temperature of ∼150°C.
5. The two cover glasses are firmly joined by the melted Nescofilm. This process can be monitored by a change in the optical properties of the Nescofilm. Gently applying pressure to the top cover glass ensures a tight seal.
6. Without delay, place the flow chamber onto the surface of a metal (e.g., aluminum) block, at room temperature, for fast cooling.
7. Mount the assembly in an appropriate holder. The process results in channels with a volume of ∼5 μl, and solutions can then be repeatedly perfused into the channels independently.

3.3. Surface Passivation and Microtubule Binding

We found that a hydrophobic surface can be very efficiently blocked using F127, a tri-block copolymer consisting of a hydrophobic poly(propylene oxide) (PPO) block in between two hydrophilic poly(ethylene glycol) (PEG) blocks. The PPO block strongly adsorbs onto the hydrophobic-rendered glass surface. The outer PEG parts form a polymer brush that is very effective in blocking protein adsorption. Stabilized microtubules are bound to the surface via anti-tubulin antibodies (see Fig. 1).

1. Perfuse Tetraspeck fluorescent microspheres into the hydrophobic-rendered glass flow cell with the assistance of a vacuum (see Notes 14, 15, and 29).
2. After a 5-min incubation, flush out excess microspheres with BRB80 (see Note 15).
3. Perfuse anti-beta-tubulin antibodies into the flow cell (see Notes 16 and 17).
4. After a 5-min incubation, flush out excess antibodies with BRB80.

5. Using F127 solution, passivate the remaining exposed surface in order to block any further nonspecific surface binding of proteins.
6. After a 10–30 min incubation, remove excess F127 with ~10 channel volumes of BRB80 (see Note 18).
7. Perfuse the solution containing microtubules (see Subheading 3.1). The incubation time depends on the desired microtubule density in the channel. Typical times range from 5 to 15 min.
8. Wash out unbound microtubules with BRB20T (see Note 19).

3.4. Imaging GFP-Labeled Kinesin-1 Motors

Due to the nature of TIRF microscopy, only fluorophores that are close to the surface are excited. Therefore, it is possible to have free GFP-labeled motors in solution and still observe single kinesin-1 molecules moving along surface-immobilized microtubules. Using this technique, it is possible to measure biophysical parameters of the motors, such as: speed, run length, and dwell time. However, the limited resolution of an optical microscope in conjunction with fast bleaching (see Notes 20–23) and low fluorescence intensity of GFP does not allow the observation of individual steps of the motor protein. This limitation can be overcome using highly efficient fluorescence probes, like Qdots, together with advanced image analysis (see Subheadings 3.5 and 3.6).

1. Perfuse ~2 channel volumes of motor solution into a channel containing surface-bound microtubules. Place the sample onto the microscope stage (see Notes 26–29).
2. Using arc lamp illumination and a rhodamine filter set, focus on the microtubules (see Note 30). Switch to laser illumination (488 nm wavelength) and a GFP filter set. In order to find the optimal TIRF angle, adjust the angle of the laser until the image becomes dark, and then turn back just until single molecules become visible in the whole field of view (see Notes 31 and 32).
3. Switch back to arc lamp illumination and rhodamine filters, move to a different field of view, and record a snapshot of the microtubule positions. Switching to laser illumination and the GFP filter set, acquire a continuous sequence of images, each with 100 ms exposure time (see Notes 33–35). An example microscope setup used to observe a kinesin-1 molecule moving along microtubules is given in the caption of Fig. 1.

3.5. Imaging Quantum Dot-Labeled Kinesin Motors

1. Mix 10 nM streptavidin-coated Qdots with 1 nM biotinylated anti-GFP antibodies. Incubate for 5 min.
2. Add 0.1–1 nM GFP-kinesin-1 to the above solution and incubate for 5 min (see Note 36).
3. Prepare the motor solution by supplementing the antifade solution from Subheading 2.4 with 4% (v/v) Qdot–kinesin solution, 100 nM ATP (if individual steps are to be resolved at 10 frames/s), and 100 μg/ml casein.
4. Continue with step 1 from Subheading 3.4 (see Notes 37 and 38).

3.6. Image Analysis: Tracking of Motors

GFP molecules with a diameter of ~2 nm or Qdots with a diameter of ~20 nm appear as point sources of light; therefore, their intensity profile can be regarded identical to the point spread function (PSF) of the imaging system. The PSF is well-approximated by a 2D Gaussian (34, 35). Therefore, fluorescent particles can be localized by fitting their camera-captured intensity profiles to a 2D Gaussian. One possibility of implementing this approach is fitting by a radially symmetric 2D Gaussian with a fixed width corresponding to the dimension of the PSF. However, we found it important to also allow radially symmetric 2D Gaussians with nonfixed widths (Eq. 1) as well as elliptical 2D Gaussians (Eq. 2). These additional degrees of freedom accommodate slightly defocused images as well as particles of larger sizes (such as fluorescent Tetraspeck beads in the 200-nm range).

$$I(x,y) = \frac{h}{2\pi\sigma^2} \times \exp\left[-\frac{(x-\hat{x})^2 + (y-\hat{y})^2}{2\sigma^2}\right] \tag{1}$$

$$I(x,y) = \frac{h}{2\pi\sigma_x\sigma_y\sqrt{1-\rho^2}} \times \exp\left[-\frac{1}{(1-\rho^2)}\left(\frac{(x-\hat{x})^2}{2\sigma_x^2} - \rho\frac{(x-\hat{x})}{\sigma_x}\frac{(y-\hat{y})}{\sigma_y} + \frac{(y-\hat{y})^2}{2\sigma_y^2}\right)\right] \tag{2}$$

Here, $I(x, y)$ denotes the intensity value at pixel position x, y; h denotes the height of the Gaussian; $\hat{x}$, $\hat{y}$ denote the position of the center of the fitting function; σ, σ_x, σ_y denote the widths; and ρ denotes the correlation coefficient determining the orientation of the Gaussian.

3.6.1. Implementation of the Tracking Routines

A tracking algorithm was developed in MATLAB (The MathWorks, Natick, MA). First, every frame is processed individually to determine the positions of all objects: (1) *Rough scanning*. Gray-scale images are converted to binary images using

predefined threshold values. Objects with intensity values above this threshold are classified as particles. (2) *Fine scanning*. The regions around the particles are fitted by Eq. 1 or 2 using estimated starting parameters. The algorithm employs a nonlinear least squares fitting routine (36, 37) and estimates the error for each parameter. Second, the fitted particle positions from individual frames are connected into tracks using an adapted feature point-tracking algorithm (38). Thereby, a cost function for four subsequent frames is calculated and includes parameters, like position, velocity, direction, or intensity. Occlusions are handled with a post-processing step, where corresponding tracks are merged automatically. The final tracking results can be displayed in an overlay with the original images offering manual verification of the fitting.

The described tracking approach was implemented in a MATLAB software package named Fluorescence Image Evaluation Software for Tracking and Analysis (FIESTA) which is freely available (39). Using FIESTA and microtubule-attached Qdots, we were able to resolve the 8 nm steps that kinesin-1 takes on the microtubule (see Fig. 2) and even smaller steps produced by two motors working collectively (29).

4. Notes

4.1. In Vitro Polymerization of Microtubules

1. As an alternative to the taxol stabilization of microtubules described in Subheading 3.1, stabilized microtubules can also be obtained by tubulin assembly in the presence of guanosine 5′-[α,β-methylene] triphosphate (GMP-CPP). For this, supplement 100 µl BRB80 with 2 µM tubulin, 4 mM $MgCl_2$, and 1 mM GMP-CPP. Allow the microtubules to assemble for ≥2 h at 37°C. Immediately before use, centrifuge the microtubule solution at 100,000 × *g* for 5 min and resuspend in BRB80 (final tubulin concentrations 0.4–4 µM). If particularly stable microtubules (lasting for several weeks at room temperature) are desired, assembled microtubules should be centrifuged immediately after polymerization and resuspended in BRB80 containing 10 µM Taxol.
2. When using chemically labeled tubulin, keep the labeling ratio as low as possible. Controls should be performed to check that labeling does not generate artifacts, such as decreased or increased run length of motor proteins on the microtubules.
3. Low temperatures cause microtubule depolymerization. Therefore, do not keep microtubules on ice or in the refrigerator.

4. Resuspending and pipetting microtubules may break them by shearing. This effect can be reduced by slow, controlled pipetting and by cutting off the pipette tip to enlarge the opening.

4.2. Preparation of the Sample Chambers

5. Piranha solution is extremely corrosive. Work with proper protective equipment and under a fume hood. Dispose of Piranha properly. Used solutions must not be stored in closed containers since gas formation continues and closed containers bare the risk of explosions (40, 41).
6. Clean glass surfaces are wetted by water. A test for cleanliness is to check whether a droplet of water spreads immediately over the complete cover glass. If a drop with a contact angle not close to 0° forms, the cover glasses are dirty!
7. Clean glass surfaces are an attractant for dirt. Therefore, it is best to use clean surfaces right away.
8. Use a clean nitrogen source for drying; use a filter on the nitrogen gas line, and clean the nitrogen gun in acetone to remove oil.
9. DDS forms insoluble crystals during storage; store upright in a sealed container at 4°C; avoid agitating the DDS in its bottle. Use a long needle and syringe to pierce the Teflon seal on the DDS bottle and draw off the required amount from the top. Using the syringe, add DDS below the TCE surface to avoid air contact. DDS vigorously reacts with water, resulting in cross-linking and crystal formation. Crystals, if present on cover glass surfaces, greatly reduce the surfaces' ability to be passivated. Store DDS under nitrogen or in a desiccator.
10. The quality of the silanization can be checked by putting a water droplet onto the glass surface and measuring its contact angle. The water contact angle should ideally be larger than 100°. Over time, the quality of silanization deteriorates. Use DDS-coated glasses within 1 week after preparation.
11. It is essential to prepare the cover glasses at all stages in as clean an environment as is possible; dry glasses in an environment free from any sources of dust; store the glass in double-sealed holders and bags; open the containers only briefly to remove glasses.
12. In place of Nescofilm, double-sided sticky tape can be used to form channels.
13. Using multiple layers of Nescofilm or tape can increase the channel volume; this decreases the surface area-to-volume ratio of the channel, mitigating the effects of any undesirable surface binding.

4.3. Surface Passivation and Microtubule Binding

14. The cover glasses used here are hydrophobic. Therefore, a vacuum line is needed to help draw the first solution into the channels. After that, filter paper can be used. Caution is needed not to introduce air bubbles into the channel because air immediately denatures any proteins on the surface.
15. The flow profile in the channel is parabolic; thus, there is slower movement of the solution near the channel walls. In order to exchange solutions in the channels thoroughly, it is necessary to flow several channel volumes of solution. Unless noted otherwise, use ~5 channel volumes.
16. Antibody concentrations should be as low as possible to not compromise surface blocking; places where antibodies are attached to the surface are not blocked by F127 in the subsequent surface passivation step.
17. As an alternative to anti-tubulin antibodies, in some cases it can be advantageous to use anti-fluorophore antibodies (42) or neutravidin (18) binding to tubulin labeled fluorescently or with biotin, respectively.
18. The channels can dry out. This damages proteins in the channel (see above). To avoid this, keep the sample chamber in a moist environment by covering it (e.g., with the lid of a pipette tip box) and adding a moist tissue. Alternatively, a drop of buffer can be added to each end of the channel, but in this case evaporation increases the salt concentration. If no additional solutions are to be perfused, channels can be sealed for long-term experiments using immersion oil or vacuum grease.
19. After the microtubules are immobilized on the surface, the low-salt buffer BRB20 is used because it increases the run length of kinesin-1.

4.4. Imaging GFP-Labeled Kinesin-1 Motors

20. In order to reduce photobleaching of fluorescent labels and to provide a reducing environment for the proteins, we add an oxygen-sequestering antifade cocktail to all our motor solutions. The antifade cocktail consists of D-glucose, glucose oxidase, catalase, and DTT. When adding these components, add the glucose oxidase last and just before actually using the motor solution, for this starts the antifade reaction. Once the antifade is complete, do not use the respective solution longer than 15–30 min. Otherwise the pH might drop significantly due to acid produced by the glucose oxidase.
21. High concentrations of glucose oxidase and catalase protein can interfere with the assay. At the same time, it is important to have high enzymatic activities in order to keep the oxygen concentration low. Therefore, it is important to always use

glucose oxidase and catalase of the highest available relative activities (i.e., units per mg).

22. For convenience and reproducibility, store all antifade components separately at −20°C in aliquots of 10 µl at a 100× concentration. Catalase and glucose oxidase are dissolved in BRB80 and snap frozen in liquid nitrogen. The frozen aliquots are stable for 6 months; when thawed and stored on ice, aliquots maintain activity for several hours. DTT is dissolved in nanopure water, stored at −20°C, and stable for ~3 months.
23. DTT can be substituted with 2-mercaptoethanol (BME). Using 10 mM BME can prolong the time until bleaching of GFP by ~50%. However, BME is less stable than DTT. Therefore, antifade solution containing BME should not be used longer than 30 min. Also, ensure that the BME stock is fresh and not oxidized by air.
24. When using motor proteins other than kinesin-1, in most cases the buffer conditions of the motor solution have to be adjusted. While BRB buffers are well-suited for microtubules and kinesin-1, our experience is that other motor proteins tend to aggregate under these conditions. In those cases, it can help to use other buffering reagents, vary the salt concentration, and add low amounts of detergents, like 0.1% Tween 20. Never add calcium and always add at least 1 mM EGTA because free calcium ions depolymerize microtubules. Also, phosphate buffers are not very suitable because phosphate is a product of the motor hydrolysis cycle.
25. The concentration of motor protein needed for single-molecule imaging greatly depends on the quality of surface blocking and the salt concentration. The flow channels have a high surface-to-volume ratio. Therefore, motor protein adsorption to the surface greatly influences the amount of free motor in solution. With increasing salt concentration, the affinity of the motor protein for the microtubule is reduced. Thus, a higher salt concentration requires more freely diffusing motor in solution.
26. To reduce thermal drift during imaging, allow the flow chamber to thermally equilibrate for about 2 min before image acquisition (sample already in contact with the immersion fluid, if non-air microscope objectives are used).
27. Another source of stage drift is airflow (e.g., in air-conditioned rooms). Shielding the microscope by a closed box (e.g., made of transparent plastic) provides a simple and effective solution.
28. The epi-fluorescence arc lamps on many microscopes generate considerable heat. To avoid unwanted sample drift, and also heating the sample itself, we do not mount our arc lamp on

the microscope and couple the light to the microscope through a multimode optical fiber.

29. To compensate for stage drift, fluorescent Tetraspeck beads can be used as drift control in the sample.
30. In order to minimize photobleaching of GFP-labeled kinesin-1, it is best to always focus on the rhodamine-labeled microtubules and then switch to the GFP filter set (start the recording immediately without refocusing). For this to work, it may be necessary to compensate for chromatic aberrations by measuring the focus offset between the GFP and the rhodamine channels and compensate for this difference before switching channels. Alternatively, a highly corrected objective, such as a Zeiss alpha Plan-Apochromat 100× oil 1.46 NA DIC (Zeiss, Jena, Germany), can be used.
31. Due to the nature of TIRF imaging, the laser comes out of the objective as a collimated beam (as opposed to a confocal microscope). Therefore, extreme precautions must be taken when the laser is on. (1) Make sure that no reflective material is above the microscope. (2) Never add or remove the sample while the laser is on. (3) Place a sheet of paper over the sample while adjusting the TIRF angle. This diffuses the laser beam while helping to see whether the laser still comes out of the objective. (4) Adjust the TIRF angle such that the laser points away from you.
32. Accurate focusing on the back focal plane can be achieved by observing the transmitted laser beam emerging from the objective some meters away on the ceiling, and adjustment of the position of the focusing lens in the TIRF condenser can then be performed.
33. For single-molecule imaging, we typically use a laser beam power of ~1–3 mW, measured as it exits the microscope objective. A higher laser power reduces the time until photo bleaching of the motors while a lower power decreases tracking accuracy.
34. A good compromise between collecting enough photons per pixel while maintaining sufficient temporal resolution is critical. We found that for many applications exposure times of 30–100 ms per frame are optimal.
35. Keep your microscope clean, and use good antireflection-coated filters and lenses. This reduces undesirable interference with reflections of the laser light from the optical components and diffraction from dust on the surfaces of optical components, which otherwise may cause a spatially nonuniform illumination due to interference fringes.

4.5. Imaging Quantum Dot-Labeled Kinesin Motors

36. When binding Qdot–streptavidin conjugates to the biotinylated antibody, make sure that there is no other source of biotin that might compete for free streptavidin-binding sites.
37. For imaging of Qdot-labeled kinesin motors, the same considerations as above apply, except that a higher laser power can be used in order to increase spatial and/or temporal resolution. We typically use a laser beam power of ~5–10 mW, measured as it exits the microscope objective.
38. Qdots are bright and photostable fluorescent emitters. Therefore they are ideally suited for high-precision nanometer tracking. One drawback of Qdots is that they blink on various timescales (ranging from submilliseconds to many seconds). Although there is no way to eliminate blinking completely, it has been reported that the use of the reducing agents BME and DTT reduces blinking dramatically (43). There are also recent reports about the synthesis of nonblinking Qdots (44–46). The localization uncertainty for GFP molecules is a magnitude higher (10–40 nm) than for Qdots (1–4 nm).

Acknowledgments

The authors would like to thank all current and former members of the Howard and Diez labs for the tremendous efforts in helping to develop the described protocols.

References

1. Sheetz, M. P., and Spudich, J. A. (1983) Movement of Myosin-Coated Fluorescent Beads on Actin Cables Invitro, *Nature* **303**, 31–35.
2. Yanagida, T., Nakase, M., Nishiyama, K., and Oosawa, F. (1984) Direct Observation of Motion of Single F-Actin Filaments in the Presence of Myosin, *Nature* **307**, 58–60.
3. Spudich, J. A., Kron, S. J., and Sheetz, M. P. (1985) Movement of Myosin-Coated Beads on Oriented Filaments Reconstituted from Purified Actin, *Nature* **315**, 584–586.
4. Svoboda, K., Schmidt, C. F., Schnapp, B. J., and Block, S. M. (1993) Direct observation of kinesin stepping by optical trapping interferometry, *Nature* **365**, 721–727.
5. Rief, M., Rock, R. S., Mehta, A. D., Mooseker, M. S., Cheney, R. E., and Spudich, J. A. (2000) Myosin-V stepping kinetics: A molecular model for processivity, *Proc. Natl. Acad. Sci. U. S. A.* **97**, 9482–9486.
6. Schnitzer, M. J., Visscher, K., and Block, S. M. (2000) Force production by single kinesin motors, *Nat. Cell. Biol.* **2**, 718–723.
7. Funatsu, T., Harada, Y., Tokunaga, M., Saito, K., and Yanagida, T. (1995) Imaging of Single Fluorescent Molecules and Individual ATP Turnovers by Single Myosin Molecules in Aqueous-Solution, *Nature* **374**, 555–559.
8. Vale, R. D., Funatsu, T., Pierce, D. W., Romberg, L., Harada, Y., and Yanagida, T. (1996) Direct observation of single kinesin molecules moving along microtubules, *Nature* **380**, 451–453.
9. Pierce, D. W., HomBooher, N., and Vale, R. D. (1997) Imaging individual green fluorescent proteins, *Nature* **388**, 338–338.

10. Helenius, J., Brouhard, G., Kalaidzidis, Y., Diez, S., and Howard, J. (2006) The depolymerizing kinesin MCAK uses lattice diffusion to rapidly target microtubule ends, *Nature* **441**, 115–119.
11. Varga, V., Helenius, J., Tanaka, K., Hyman, A. A., Tanaka, T. U., and Howard, J. (2006) Yeast kinesin-8 depolymerizes microtubules in a length-dependent manner, *Nat. Cell. Biol.* **8**, 957–960.
12. Bieling, P., Laan, L., Schek, H., Munteanu, E. L., Sandblad, L., Dogterom, M., Brunner, D., and Surrey, T. (2007) Reconstitution of a microtubule plus-end tracking system in vitro, *Nature* **450**, 1100–1105.
13. Brouhard, G. J., Stear, J. H., Noetzel, T. L., Al-Bassam, J., Kinoshita, K., Harrison, S. C., Howard, J., and Hyman, A. A. (2008) XMAP215 is a processive microtubule polymerase, *Cell* **132**, 79–88.
14. Fink, G., Hajdo, L., Skowronek, K. J., Reuther, C., Kasprzak, A. A., and Diez, S. (2009) The mitotic kinesin-14 Ncd drives directional microtubule-microtubule sliding, *Nat. Cell. Biol.* **11**, 717–723.
15. Varga, V., Leduc, C., Bormuth, V., Diez, S., and Howard, J. (2009) Kinesin-8 motors act cooperatively to mediate length-dependent microtubule depolymerization, *Cell* **138**, 1174–1183.
16. Seitz, A., Kojima, H., Oiwa, K., Mandelkow, E. M., Song, Y. H., and Mandelkow, E. (2002) Single-molecule investigation of the interference between kinesin, tau and MAP2c, *EMBO J.* **21**, 4896–4905.
17. Dixit, R., Ross, J. L., Goldman, Y. E., and Holzbaur, E. L. (2008) Differential regulation of dynein and kinesin motor proteins by tau, *Science* **319**, 1086–1089.
18. Telley, I. A., Bieling, P., and Surrey, T. (2009) Obstacles on the microtubule reduce the processivity of Kinesin-1 in a minimal in vitro system and in cell extract, *Biophys. J.* **96**, 3341–3353.
19. Korten, T., and Diez, S. (2008) Setting up roadblocks for kinesin-1: mechanism for the selective speed control of cargo carrying microtubules, *Lab Chip* **8**, 1441–1447.
20. Axelrod, D., Burghardt, T. P., and Thompson, N. L. (1984) Total internal reflection fluorescence, *Annu. Rev. Biophys. Bioeng.* **13**, 247–268.
21. Thompson, N. L., and Steele, B. L. (2007) Total internal reflection with fluorescence correlation spectroscopy, *Nat. Protoc.* **2**, 878–890.
22. Gell, C., Berndt, M., Enderlein, J., and Diez, S. (2009) TIRF microscopy evanescent field calibration using tilted fluorescent microtubules, *J. Microsc.* **234**, 38–46.
23. Gell, C., Brockwell, D. J., and Smith, D. A. M. (2006) *Handbook of Single Molecule Fluorescence Spectroscopy*, Oxford University Press, Oxford, UK.
24. Gelles, J., Schnapp, B. J., and Sheetz, M. P. (1988) Tracking kinesin-driven movements with nanometre-scale precision, *Nature* **331**, 450–453.
25. Anderson, C. M., Georgiou, G. N., Morrison, I. E., Stevenson, G. V., and Cherry, R. J. (1992) Tracking of cell surface receptors by fluorescence digital imaging microscopy using a charge-coupled device camera. Low-density lipoprotein and influenza virus receptor mobility at 4 degrees C, *J. Cell Sci.* **101 (Pt 2)**, 415–425.
26. Hua, W., Young, E. C., Fleming, M. L., and Gelles, J. (1997) Coupling of kinesin steps to ATP hydrolysis, *Nature* **388**, 390–393.
27. Yildiz, A., Forkey, J. N., McKinney, S. A., Ha, T., Goldman, Y. E., and Selvin, P. R. (2003) Myosin V walks hand-over-hand: single fluorophore imaging with 1.5-nm localization, *Science* **300**, 2061–2065.
28. Nitzsche, B., Ruhnow, F., and Diez, S. (2008) Quantum-dot-assisted characterization of microtubule rotations during cargo transport, *Nature Nanotechnology* **3**, 552–556.
29. Leduc, C., Ruhnow, F., Howard, J., and Diez, S. (2007) Detection of fractional steps in cargo movement by the collective operation of kinesin-1 motors, *Proc. Natl. Acad. Sci. U. S. A.* **104**, 10847–10852.
30. Rogers, K. R., Weiss, S., Crevel, I., Brophy, P. J., Geeves, M., and Cross, R. (2001) KIF1D is a fast non-processive kinesin that demonstrates novel K-loop-dependent mechanochemistry, *EMBO J.* **20**, 5101–5113.
31. Meurer-Grob, P., Kasparian, J., and Wade, R. H. (2001) Microtubule structure at improved resolution, *Biochemistry (Mosc)*. **40**, 8000–8008.
32. Pierson, G. B., Burton, P. R., and Himes, R. H. (1978) Alterations in number of protofilaments in microtubules assembled in vitro, *J. Cell Biol.* **76**, 223–228.
33. Ray, S., Meyhofer, E., Milligan, R. A., and Howard, J. (1993) Kinesin follows the microtubule's protofilament axis, *J. Cell Biol.* **121**, 1083–1093.
34. Cheezum, M. K., Walker, W. F., and Guilford, W. H. (2001) Quantitative comparison of algorithms for tracking single fluorescent particles, *Biophys. J.* **81**, 2378–2388.

35. Thompson, R. E., Larson, D. R., and Webb, W. W. (2002) Precise nanometer localization analysis for individual fluorescent probes, *Biophys. J.* **82**, 2775–2783.
36. Moré, J. J. (1977) The Levenberg-Marquardt Algorithm: Implementation and Theory, in *Numer. Anal.* (Watson, G. A., Ed.), pp 105–116, Springer Verlag.
37. Coleman, T. F., and Li, Y. (1994) On the Convergence of Reflective Newton Methods for Large-Scale Nonlinear Minimization Subject to Bounds, *Math. Program.* **67**, 189–224.
38. Chetverikov, D., and Verestóy, J. (1999) Feature Point Tracking for Incomplete Trajectories, *Computing* **62**, 321–338.
39. Ruhnow, F., Zwicker, D., and Diez, S. (2011) Tracking single particles and elongated filaments with nanometer precision, *Biophys. J.* **100,** 2820–2828.
40. Dobbs, D. A., Bergman, R. G., and Theopold, K. H. (1990) Piranha Solution Explosion, *Chem. Eng. News* **68**, 2–2.
41. Erickson, C. V. (1990) Piranha Solution Explosions, *Chem. Eng. News* **68**, 2–2.
42. Reuther, C., Hajdo, L., Tucker, R., Kasprzak, A. A., and Diez, S. (2006) Biotemplated nanopatterning of planar surfaces with molecular motors, *Nano Lett* **6**, 2177–2183.
43. Hohng, S., and Ha, T. (2004) Near-complete suppression of quantum dot blinking in ambient conditions, *J. Am. Chem. Soc.* **126**, 1324–1325.
44. Chen, Y., Vela, J., Htoon, H., Casson, J. L., Werder, D. J., Bussian, D. A., Klimov, V. I., and Hollingsworth, J. A. (2008) "Giant" multishell CdSe nanocrystal quantum dots with suppressed blinking, *J. Am. Chem. Soc.* **130**, 5026–5027.
45. Mahler, B., Spinicelli, P., Buil, S., Quelin, X., Hermier, J. P., and Dubertret, B. (2008) Towards non-blinking colloidal quantum dots, *Nat. Mat.* **7**, 659–664.
46. Wang, X. Y., Ren, X. F., Kahen, K., Hahn, M. A., Rajeswaran, M., Maccagnano-Zacher, S., Silcox, J., Cragg, G. E., Efros, A. L., and Krauss, T. D. (2009) Non-blinking semiconductor nanocrystals, *Nature* **459**, 686–689.
47. Kerssemakers, J. W., Munteanu, E. L., Laan, L., Noetzel, T. L., Janson, M. E., and Dogterom, M. (2006) Assembly dynamics of microtubules at molecular resolution, *Nature* **442**, 709–712.